questions concern the mechanism of transfer, the frequent co-insertion of non-contiguous mitochondrial inserts and the presence of mitochondrial insertions in the vicinity of LTRs and tRNA genes. □

Methods

Experimental methods

The two haploid strains used are derivatives of FYBL2-5D (*MAT*-α, *ura3Δ851*, *leu2Δ1*, *trp1Δ63*), in which *YKL222c* (position 3507–5621) or *YKR098c* (position 632659–634809) have been replaced by the *URA3* I-*Sce*I cassette. Both strains are isogenic to the FY1679 (S288C) strain whose nuclear genome has been sequenced[26], except for the markers indicated. Both mutants retained the wild-type phenotype of the haploid cell. Yeast cells were transformed with the replicative I-*Sce*I expression plasmid, pPEX7, by the lithium acetate method. Analysis of repair was performed by PCR directly on cells using 20-mer oligonucleotides whose 5′-end coordinates are 2725 and 6106 for FYBL2-5D *Δykl222c*::*URA3* I-*Sce*I, and 632491 and 633481 for FYBL2-5D *Δykr098c*::*URA3* I-*Sce*I (see Fig. 1). In both cases the primer distal to the centromere was biotinylated. Polymerase chain reaction products were separated on 1.5% agarose gels. Under these conditions insertions or deletions of at least 50 bp are detectable. These PCR-amplified DNA fragments were cut out from the gel and purified with QIAquick PCR Purification kit (Qiagen). The appropriate single-strand DNA was separated with streptavidine and then sequenced.

The *Δyme1* mutant of the strain FYBL2-5D *Δykr098c*::*URA3* I-*Sce*I was obtained with the one-step gene-disruption technique by replacing *YPR024w* (*YME1*) with the KANMX module[29]. The presence of the KANMX module instead of *YPR024w* was molecularly checked by PCR amplification of the specific fragment and by the restriction pattern of the amplified fragment with different restriction enzymes. As described for the *yme1* mutant[19], the double mutant *Δyme1*, *Δykr098c* constructed here did not form ρ^- or ρ^0 colonies and was unable to grow on glucose at 14 °C and on glycerol at 37 °C. The ρ^- and ρ^0 mutants of the FYBL2-5D *Δykr098c* strain were obtained as described[30]. By definition, ρ^- strains retain only a fraction of the wild-type mitochondrial genome, often in an amplified and rearranged configuration, and ρ^0 strains have no mitochondrial DNA. The ρ^- mutant was partially characterized by PCR amplification of short mitochondrial sequences and by Southern blot analysis using purified mitochondrial DNA digested with different restriction enzymes. These last two techniques were also used to reveal the absence of mitochondrial DNA in the ρ^0 mutants.

DNA sequence comparison

Sequences of PCR inserts were compared first with the Genbank and EMBL databases and, subsequently with the mitochondrial yeast genome[4] using BLAST2. The systematic sequence comparison between the mitochondrial and the nuclear genome of FY1679 was performed using BLAST2. The nuclear yeast genome sequence was retrieved from MIPS (http://speedy.mips.biochem.mpg.de/mips/yeast) on 23 December 1998. The sequence of the mitochondrial genome of strain FY1679 was kindly provided by F. Foury[4]. Mitochondrial DNA sequence was fragmented into 200-bp-long sequences to serve as query. Two different fragmentations shifted by 100 bp with respect to each other were used. Defined mitochondrial sequences matching the nuclear genome were then compared once more with the nuclear genome and classified by increasing BLAST2 probability scores. Sequences with probability $\leqslant 6.0 \times 10^{-3}$ are shown in Table 2 and discussed in the text.

In addition to this first group of sequences, 137 other short mitochondrial sequences (18–21 bp in length) have 100% identity with nuclear sequences. They were excluded from the previous list based exclusively on BLAST scores but have statistical significance ($<10^{-3}$) if the length of the fragment, the size of the nuclear genome and the nucleotide composition of both the mitochondrial and the nuclear genome are taken into account. These sequences originate from both coding and non-coding regions of the mitochondrial genome. Although statistically significant, the fact that these sequences have such a small size and that a third of them are present in coding regions of chromosomes (compared with only 9% for the longer sequences) suggests that some of these may correspond to random coincidence rather than actual transfer. These sequences have not been taken into consideration in our conservative analysis.

Received 7 July; accepted 19 August 1999.

1. Margulis, L. in *Origin of Eukaryotic Cells* (Yale University Press, New Haven and London, 1970).
2. Perna, N. T. & Kocher, T. D. Molecular fossils in the nucleus. *Curr. Biol.* **6,** 128–129 (1996).
3. Thorsness, P. E. & Weber, E. R. Escape and migration of nucleic acids between chloroplast, mitochondria, and the nucleus. *Int. Rev. Cytol.* **165,** 207–231 (1996).
4. Foury, F., Roganti, T., Lecrenier, N. & Purnelle, B. The complete sequence of the mitochondrial genome of *Saccharomyces cerevisiae*. *FEBS Lett.* **440,** 325–331 (1998).
5. Resnick, M. A. & Martin, P. The repair of double-strand breaks in the nuclear DNA of *Saccharomyces cerevisiae* and its genetic control. *Mol. Gen. Genet.* **143,** 119–129 (1976).
6. Kramer, K. M., Brock, J. A., Bloom, K., Moor, J. K. & Haber, J. E. Two different types of double-strand breaks in *Saccharomyces cerevisiae* are repaired by similar RAD52-independent, nonhomologous recombination events. *Mol. Cell. Biol.* **14,** 1293–1301 (1994).
7. Fairhead, C., Llorente, B., Denis, F., Soler, M. & Dujon, B. New vectors for combinatorial deletions in yeast chromosomes and for gap-repair cloning using 'split-marker' recombination. *Yeast* **12,** 1439–1457 (1996).
8. Teng, S.-C., Kim, B. & Gabriel, A. Retrotransposon reverse-transcriptase-mediated repair of chromosomal breaks. *Nature* **383,** 641–644 (1996).
9. Moore, K. J. & Haber, J. E. Capture of retrotransposon DNA at the sites of chromosomal double-strand breaks. *Nature* **383,** 644–646 (1996).
10. Fairhead, C., Thierry, A., Denis, F., Eck, M. & Dujon, B. 'Mass-murder' of ORFs from three regions of chromosome XI from *Saccharomyces cerevisiae*. *Gene* **223,** 33–46 (1998).
11. Fairhead, C. & Dujon, B. Consequence of double-stranded breaks in yeast chromosomes: death or homozygosis. *Mol. Gen. Genet.* **240,** 170–180 (1993).
12. de Zamaroczy, M. & Bernardi, G. The primary structure of the mitochondrial genome of *Saccharomyces cerevisiae*—a review. *Gene* **47,** 155–157 (1986).
13. Roth, D. B. & Wilson, J. H. Nonhomologous recombination in mammalian cells: role for short sequence homologies in the joining reaction. *Mol. Cell. Biol.* **6,** 4295–4304 (1986).
14. Roth, D. & Wilson, J. in *Genetic Recombination* (eds Kucherlapati, R. & Smith, G. R.) 621–653 (American Society for Microbiology, Washington DC, 1988).
15. Gorbunova, V. & Levy, A. A. Non-homologous DNA end joining in plant cells is associated with deletions and filler DNA insertions. *Nucleic Acids Res.* **25,** 4650–4657 (1997).
16. Sargent, R. G., Brenneman, M. A. & Wilson, J. M. Repair of site-specific double-strand breaks in a mammalian chromosome by homologous and illegitimate recombination. *Mol. Cell. Biol.* **17,** 267–277 (1997).
17. Schiestl, R. H., Domiska, M. & Petes, T. D. Transformation of *Saccharomyces cerevisiae* with nonhomologous DNA: illegitimate integration of transforming DNA into yeast chromosomes and *in vivo* ligation of transforming DNA to mitochondrial sequences. *Mol. Cell. Biol.* **13,** 2697–2705 (1993).
18. Thorsness, P. E. & Fox, T. D. Escape of DNA from mitochondria to the nucleus in *Saccharomyces cerevisiae*. *Nature* **346,** 376–379 (1990).
19. Thorsness, P. E. & Fox, T. D. Nuclear mutations in *Saccharomyces cerevisiae* that affect the escape of DNA from mitochondria to the nucleus. *Genetics* **134,** 21–28 (1993).
20. Byers, B. in *The Molecular Biology of the Yeast* Saccharomyces cerevisiae (eds Strathern, J. N., Jones, E. W. & Broach, J. R.) 59–96 (Cold Spring Harbor Laboratory, Cold Spring Harbor, New York, 1981).
21. Farrelly, F. & Butow, R. Rearranged mitochondrial genes in the yeast nuclear genome. *Nature* **301,** 296–301 (1983).
22. Louis, E. J. & Haber, J. E. Evolutionarily recent transfer of a group I mitochondrial intron to telomere regions in *Saccharomyces cerevisiae*. *Curr. Genet.* **20,** 411–415 (1991).
23. Blanchard, J. L. & Schmidt, G. W. Mitochondrial DNA migration events in yeast and humans: integration by a common end-joining mechanism and alternative perspectives on nucleotide substitution patterns. *Mol. Biol. Evol.* **13,** 537–548 (1996).
24. Churcher, C. *et al.* The nucleotide sequence of *Saccharomyces cerevisiae* chromosome IX. *Nature* **387,** (Suppl) 84–87 (1997).
25. Feuermann, M., De Montigny, J., Potier, S. & Souciet, J.-L. The characterization of two new clusters of duplicated genes suggests a 'lego' organization of the yeast *Saccharomyces cerevisiae* chromosomes. *Yeast* **13,** 861–869 (1997).
26. Goffeau, A. *et al.* Life with 6000 genes. *Science* **274,** 546–567 (1996).
27. Baudat, F. & Nicolas, A. Clustering of meiotic double-strand breaks on yeast chromosome III. *Proc. Natl Acad. Sci. USA* **94,** 5213–5218 (1997).
28. Wolfe, K. M. & Shields, D. C. Molecular evidence for an ancient duplication of the entire yeast genome. *Nature* **387,** 708–713 (1997).
29. Wach, A., Brachat, A., Pohlmann, R. & Philippsen, P. New heterologous modules for classical or PCR based gene-disruptions in *Saccharomyces cerevisiae*. *Yeast* **10,** 1793–1808 (1994).
30. Hauswirth, W. W., Lim, L. O., Dujon, B. & Turner, G. in *Mitochondria. A Practical Approach* (eds Darley-Usmar, V. M., Rickwood, D. & Wilson, M. T.) 171–242 (IRL Press, Oxford, 1987).

Acknowledgements

We thank F. Foury for having provided the entire mitochondrial sequence of *S. cerevisiae*, D. Alexandraki for the yeast strain *Δykl222c*, A. Harrington for purified mitochondrial DNA, A. Thierry for the *Δyme1* strategy, F. Tekaia and A. Perrin for bioinformatics, M. Buckingham and T. Pugsley for comments on the manuscript and Henri Buc in whose laboratory some of these experiments were performed. This work was supported by a grant from the European Commission (EUROFAN). B.D. is a member of Institut Universitaire de France.

Correspondence and requests for materials should be addressed to M.R. (e-mail: mricch@pasteur.fr).

Mechanical unfolding intermediates in titin modules

Piotr E. Marszalek*, Hui Lu†, Hongbin Li*, Mariano Carrion-Vazquez*, Andres F. Oberhauser*, Klaus Schulten† & Julio M. Fernandez*

** Department of Physiology and Biophysics, Mayo Foundation, Rochester, Minnesota 55905, USA*
† Beckman Institute for Advanced Science and Technology, University of Illinois at Urbana-Champaign, Urbana, Illinois 61801, USA

The modular protein titin, which is responsible for the passive elasticity of muscle, is subjected to stretching forces. Previous work on the experimental elongation of single titin molecules has suggested that force causes consecutive unfolding of each domain in an all-or-none fashion[1–6]. To avoid problems associated with the heterogeneity of the modular, naturally occurring titin, we

engineered single proteins to have multiple copies of single immunoglobulin domains of human cardiac titin[7]. Here we report the elongation of these molecules using the atomic force microscope. We find an abrupt extension of each domain by ~7 Å before the first unfolding event. This fast initial extension before a full unfolding event produces a reversible 'unfolding intermediate'. Steered molecular dynamics[8,9] simulations show that the rupture of a pair of hydrogen bonds near the amino terminus of the protein domain causes an extension of about 6 Å, which is in good agreement with our observations. Disruption of these hydrogen bonds by site-directed mutagenesis eliminates the unfolding intermediate. The unfolding intermediate extends titin domains by ~15% of their slack length, and is therefore likely to be an important previously unrecognized component of titin elasticity.

The complex mechanical design of the elastic protein titin is still not understood[1–7,10–20]. Recent *in vitro* studies using optical tweezers and atomic force microscopy (AFM) have revealed at least two components, where titin elasticity is governed by the entropic behaviour of its segments and the unravelling of its folded domains[2,3,5]. The force–extension relationship of titin was explained by models of simple entropic elasticity[2,3,5,7] in which module unfolding increased the contour length of the protein in a stepwise fashion[2,5]. In the experiments using an atomic force microscope (AFM), extension of titin domains generated a force–extension relationship with a characteristic sawtooth pattern of equally spaced peaks that result from the sequential unfolding of its modules[5,7]. In these recordings, the force–extension relationship of titin leading up to an unfolding event is described by the worm-like chain (WLC) model of polymer elasticity[2,3,5–7]. However, close examination of the rising phases of the force peaks shows that they deviate from the shape predicted by the WLC model, raising the possibility that there are additional components in the elasticity of titin modules which have been missed. This is particularly evident in the rising phase of the first force peak which shows the elasticity of the protein before any unfolding event[21].

Figure 1a shows that the force–extension curve of a native titin fragment strongly deviates from the expected entropic elasticity (WLC), revealing a pronounced 'hump' that tends to disappear on unfolding of all the modules. Native titin is a highly heterogeneous polymer, and therefore it is difficult to relate its elastic properties to individual structural elements. Hence, to examine the elastic components of titin modules at high resolution we engineered polyproteins composed of identical tandem repeats of either the I28 module ($I28_8$) or the I27 module ($I27_{12}$; ref. 7) of human cardiac titin (see Methods). Stretching a polyprotein with identical repeats of a module linearly amplifies the mechanical features of the protein module, revealing fine mechanical details at high resolution.

Force–extension curves for the $I28_8$ and $I27_{12}$ polyproteins showed the characteristic sawtooth patterns, corresponding to the sequential unfolding of their modules (Fig. 1b–d). Fits of the WLC to the force–extension curves leading up to the first peak (Fig. 1b–d; thin lines on the first peak) show a large deviation from simple entropic elasticity that becomes apparent at 108 ± 19 pN (I27, $n = 87$) and 151 ± 16 pN (I28, $n = 30$), well before the unfolding events occur (210 ± 27 pN, I27, $n = 87$; 264 ± 49 pN, I28, $n = 30$). When the force reaches ~100–150 pN (Fig. 1b–d), the slope of the force–extension curve decreases sharply creating the shape of a 'hump' that deviates from the line predicted by the WLC model. After this deviation, the slope of the curve increases again, after which the force reaches a maximum of about 200–300 pN where domain unfolding occurs.

Abrupt slope changes in the force–extension curve of a molecule, such as those shown in Fig. 1b–d, have been observed in polysaccharides and have been shown to correspond to force-induced transitions that elongate the molecule by a small amount[6,22]. Hence, it is likely that the 'hump' observed in the force–extension curves of

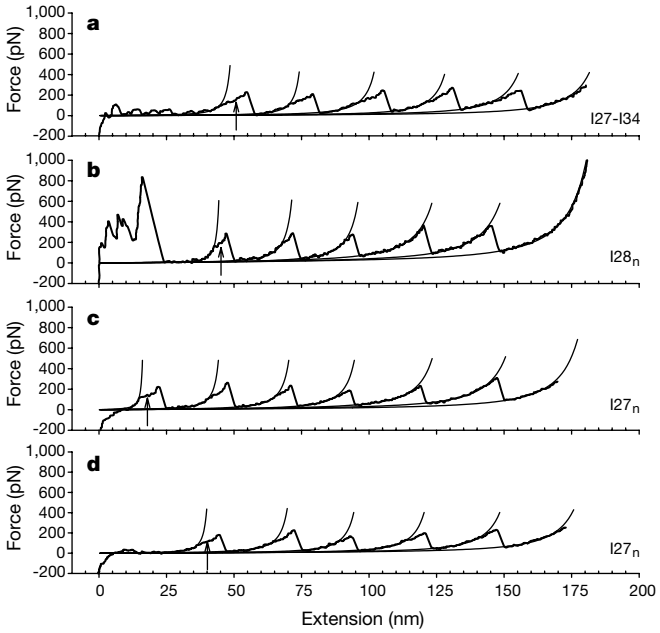

Figure 1 Force peaks corresponding to the sequential unfolding of immunoglobulin-like domains of human cardiac titin, showing large hump-like deviations from the WLC model of entropic elasticity (arrows). **a**, Force–extension curve for a fragment of human cardiac I band titin encompassing the immunoglobulin-like domains I27 to I34 (refs 5, 21). **b**–**d**, Force–extension relationship for a polyprotein constructed from tandem repeats of the I28 module (**b**) and the I27 module (**c**, **d**). In all cases, the experimental data display a prominent hump in the rising phase of the initial force peaks and therefore can not be fitted with the WLC model (thin lines).

$I28_8$ and $I27_{12}$ corresponds to a previously undetected force-driven transition that elongates folded modules by a small amount at forces of 150 pN (I28) and 100 pN (I27). This elongation is a property of folded modules only. The hump in the force–extension relationship is most evident in the first peak, but it diminishes gradually with module unfolding and disappears completely when all the modules have unfolded and the protein is fully extended (Fig. 1; thin lines on the last peak).

The structure of the I27 module of titin is known, and its mechanical topology has been examined by molecular dynamics[23] and single-molecule AFM[7]. Thus, the I27 module is ideal to examine the molecular origin of the 'hump'. In Fig. 2, we analyse in detail the transitional extension observed at ~100 pN in the $I27_{12}$ polyprotein. We measured the width of this transition as a contour length increment, ΔL_c, obtained by fitting the WLC model before and after the transition, as shown in Fig. 2a. These measurements were done on the transition observed in the first peak where the transition is most prominent. Although the $I27_{12}$ polyprotein is engineered with 12 tandem modules, the AFM tip rarely picks up the protein from its termini. Hence, the AFM tip picks up proteins of various lengths, from very short proteins (2 modules long) up to their maximum length (12 modules long). We found that ΔL_c, measured in the first unfolding peak, increases linearly with the total number of folded modules of the polyprotein fragments picked by the AFM tip (Fig. 2b). A linear regression of the data in Fig. 2b gives a slope of 6.6 Å per module.

This result indicates that at ~100 pN, a folded domain undergoes a transitional extension of 6.6 Å; this extension contrasts with the much larger 284 Å extension caused by the full unfolding of the I27 module observed at ~200 pN (ref. 7). Figure 2c shows a histogram of the force at which the first transitional extension is observed compared with the unfolding force. A gaussian fit of the data (Fig. 2c; solid lines) gives a force of 108 pN for the small transitional extension, and 210 pN for the full unfolding event ($n = 87$).

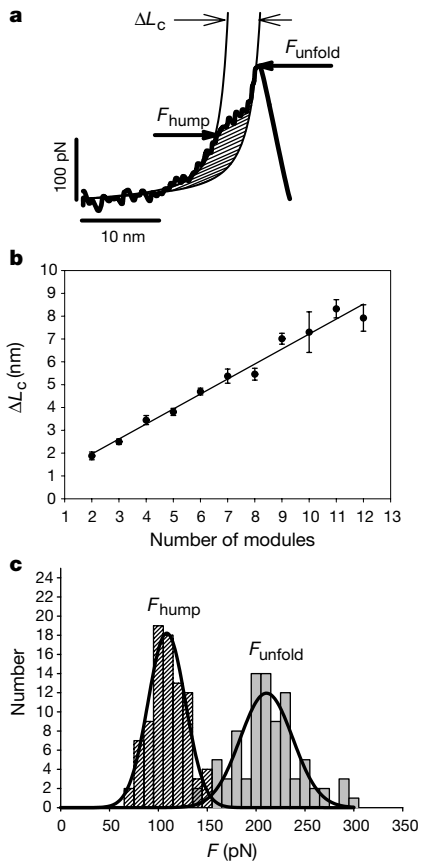

Figure 2 The size of the hump-like deviation depends linearly on the number of folded modules. **a**, Plot of the first force peak of a sawtooth pattern. The hump begins at a force, F_{hump}, that is smaller than the force required to completely unfold the module, F_{unfold}. The thin lines are fits of the WLC model to the data before and after the hump. The contour length of the second fit is $\Delta L_c = 46.5$ Å longer than the one before the hump. The dashed area represents the work done by extending the protein through its intermediate. **b**, Relationship between ΔL_c (measured in the first unfolding peak) and the number of modules in the stretched tandem repeat. The solid line is a linear regression to the data with the slope: 6.6 Å per module ($r^2 = 0.98$, $n = 87$). The bars indicate standard errors. **c**, Histogram of F_{hump} and F_{unfold}. Gaussian fits (solid lines) to the data give average values of $F_{hump} = 108$ pN and $F_{unfold} = 210$ pN ($n = 87$). The pulling speed was 0.3–0.5 nm ms^{-1}.

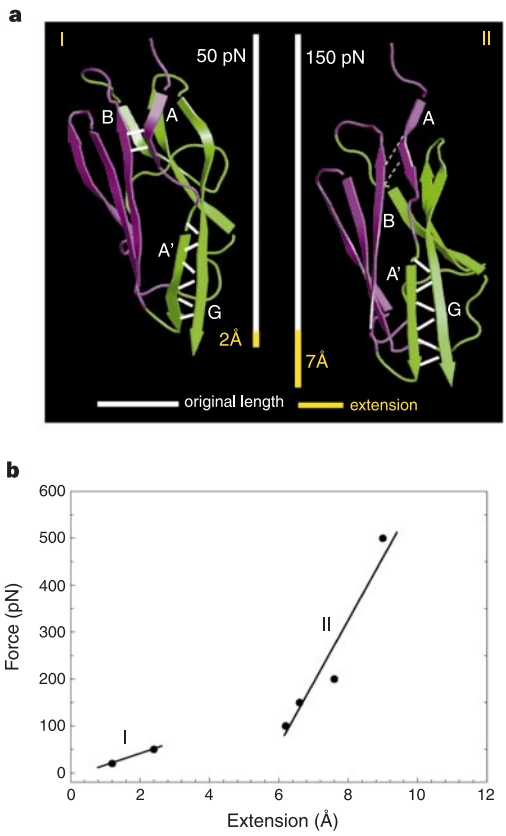

Figure 3 Steered molecular dynamics simulations of I27 extensibility under constant force. **a**, 'Snapshots' of the structure of the I27 module simulated at a force of 50 pN (I, at 1 ns) and 150 pN (II, at 1 ns). At 50 pN the hydrogen bonds between strands A and B are maintained, whereas at 150 pN they are broken. **b**, I27 force–extension relationship obtained from the simulations. The discontinuity observed between 50 and 100 pN corresponds to an abrupt extension of the module by 4–7 Å caused by the rupture of the AB hydrogen bonds, and the subsequent extension of the partially freed polypeptide segment. Figure generated using the program VMD[30].

However, the unfolding forces are dependent on the rate at which the protein is pulled[5–7,24]. Hence it is likely that the small transitional extension observed here may also occur at much lower forces.

Although the small transitional extension of the I27 module is most prominent in the first unfolding peak of the force–extension curve, this transition is also observed in consecutive peaks, albeit with decreasing amplitude (Fig. 1). These observations put together suggest that the transition observed in the first peak corresponds to the accumulated transitional extension of all the folded domains. The reappearance of a progressively smaller transition in consecutive peaks suggests that the transition is reversible upon relaxation of the force (peak to trough transition), and that a small transitional extension of the modules that remain folded occurs again at a force of ~100 pN. We estimate that the refolding rate of the small transitional extension must be at least 25 s^{-1} in order to fully recover between unfolding events (Fig. 1). This fast refolding rate contrasts with the much slower refolding observed after full unfolding of the I27 module (~1 s^{-1}; ref. 7).

Steered molecular dynamics (SMD) simulations of the forced extension of the I27 module predict that the mechanical resistance in this module arises from a patch of six hydrogen bonds bridging the A′ and G β-strands (Fig. 3a). According to these simulations, the simultaneous rupture of this patch of hydrogen bonds is the critical event that allows the full unravelling of the module under an applied force[23]. These simulations showed that the rupture of the two hydrogen bonds bridging the A and B β-strands was a minor event that preceded the rupture of the A′G patch[23]. We examined whether the small extension that precedes the main unfolding event was due to the rupture of two hydrogen bonds bridging the AB β-strands (K6-E24). For this purpose, SMD simulations were performed in which forces of 20, 50, 100, 150, 200 and 500 pN were applied, each for 1 ns, to the termini of a single I27 domain. Upon application of these forces, the I27 domain extended within less than 200 ps to a quasi-equilibrium value that is plotted in Fig. 3b. Full unfolding within the 1-ns time window was observed only for the strongest force (500 pN). At forces of less than 50 pN the I27 module was forced to extend by ~2 Å, whereas for forces larger than 100 pN the quasi-stationary extensions ranged from 6 to 9 Å. Analysis of the SMD trajectories showed that at forces of 20 pN and 50 pN the hydrogen bonds between the A and B β-strands are maintained (Fig. 3b, line I) and that the 2-Å extension arising in this case is due to straightening of the terminal residues. At larger forces these hydrogen bonds break (Fig. 3b, line II), producing a discontinuous extension from 2 Å at lower forces to an additional 4–7 Å (at forces ≥100 pN; Fig. 3b). The discontinuous elongation caused by the rupture of these hydrogen bonds is in good agreement with the 6.6-Å elongation observed with the AFM. This event occurs at low force and precedes the full unravelling of the I27 module. Furthermore, an estimate of the mechanical work done to extend

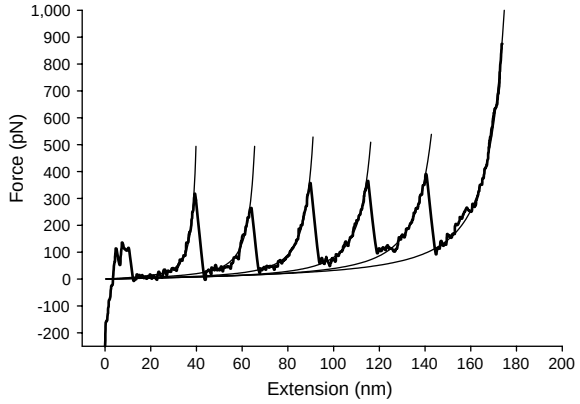

Figure 4 Removal of the deviation from the WLC model by introducing a point mutation in the I27 polyprotein ($I27_9$-K6P). The point mutation substituted lysine 6 by a proline. This proline in position 6 disrupts the two critical hydrogen bonds that link the A and B β-strands together. In contrast to the wild-type form of the I27 module, the rising phase of all force peaks measured from the $I27_9$-K6P protein closely follows the WLC model.

the modules at low force gives a value of 10.1 ± 0.63 kcal per mol per module (Fig. 2a, hatched area) which agrees well with the work required to rupture a pair of hydrogen bonds[25].

These observations strongly suggest that the unfolding intermediate that we observe during the extension of the I27 module corresponds to the rupture of the pair of hydrogen bonds bridging the A and B β-strands of the I27 module. To verify this view, we engineered a point mutant polyprotein ($I27_9$-K6P; 9 repeats of a mutant I27 module where lysine in position 6 was replaced by a proline) where the mutation interferes with the formation of these hydrogen bonds. Figure 4 shows a force–extension curve for the ($I27_9$-K6P) polyprotein. The figure shows that, in contrast to the wild-type form, the mutant polyprotein does not show deviations from the WLC model. Hence, introduction of the K6P mutation eliminates the unfolding intermediate that we have described.

A folded I27 module has a length of 44 Å, as determined by NMR[13]. We have shown that a force of ~100 pN can extend the module by 6.6 Å without causing full domain unfolding. This rapidly reversible unfolding intermediate corresponds to an extension of a titin module by 15% of its resting length. Our data therefore provide direct evidence for a new source of extensibility in human cardiac titin, caused by a force-driven conformational change in its immunoglobulin domains. □

Methods

Protein engineering

We constructed polyproteins containing 12 direct tandem repeats of a single immunoglobulin domain no. 27, and 8 tandem repeats of a single immunoglobulin domain no. 28 from the I band of human cardiac titin, according to methods described elsewhere[7]. We also expressed and purified the I27-I34 construct of human cardiac titin synthesized elsewhere[5]. The I27-K6P point mutation monomer was generated by polymerase chain reaction using mutagenic primers. All these recombinant proteins have two Cys residues in their carboxy terminus to facilitate the attachment of the molecules to the gold-coated coverslips.

Force spectroscopy of single proteins

Our custom-made AFM apparatus and its mode of operation have been described[26]. Calibration of the spring constant of each individual cantilever was done in solution using the equipartition theorem as described in ref. 27. The proteins were suspended in PBS buffer at a concentration of ~10 μg ml^{-1} and adsorbed onto freshly evaporated gold coverslips. For the analysis of the polyproteins, we chose only recordings showing a sawtooth force pattern that ended with a high-force peak that corresponds to stretching a fully denatured protein (all modules unfolded). This allowed us to count the number of modules within the fragment of the protein that were actually stretched.

Steered molecular dynamics simulation

The steered molecular dynamics (SMD) simulations of I27 were performed with the programs NAMD[28] and XPLOR[29] with the CHARMm22 (ref. 29) force field. The structure of I27 has been reported[13] and is available elsewhere (Brookhaven PDB databank; PDB code 1TIT). The structure was solvated in water and equilibrated following the procedure described elsewhere[23]. SMD simulations with constant forces were performed by fixing one terminus of the domain and applying the force to the other terminus. The direction of the force was chosen along the vector from the N terminus to the C terminus. The constant stretching force F (pN) was determined by adding a harmonic potential between the C terminus and a point relatively far away (400 nm) from it along the force direction with the spring constant set to F(pN)/400(nm). The fluctuation of the magnitude of the force is less than 0.2%. The simulation adopted a timestep of 1 fs, a uniform dielectric constant of 1, and a cut-off of Coulomb and van der Waals interactions with switching function starting at a distance of 10 Å and reaching zero at 13 Å. Simulation time, 1 ns.

Received 26 April; accepted 18 August 1999.

1. Erickson, H. P. Stretching single protein molecules: titin is a weird spring. *Science* **276,** 1090–1092 (1997).
2. Tskhovrebova, L., Trinick, J., Sleep, J. A. & Simmons, R. M. Elasticity and unfolding of single molecules of the giant muscle protein titin. *Nature* **387,** 308–312 (1997).
3. Kellermayer, M. S. Z., Smith, S. B., Granzier, H. L. & Bustamante, C. Folding-unfolding transitions in single titin molecules characterized with laser tweezers. *Science* **276,** 1112–1116 (1997).
4. Kellermayer, M. S. Z., Smith, S. B., Bustamante, C. & Granzier, H. L. Complete unfolding of the titin molecule under external force. *J. Struct. Biol.* **122,** 197–205 (1998).
5. Rief, M., Gautel, M., Oesterhelt, F., Fernandez, J. M. & Gaub, H. E. Reversible unfolding of individual titin immunoglobulin domains by AFM. *Science* **276,** 1109–1112 (1997).
6. Rief, M., Fernandez, J. M. & Gaub, H. E. Elastically coupled two-level-systems as a model for biopolymer extensibility. *Phys. Rev. Lett.* **81,** 4764–4767 (1998).
7. Carrion-Vazquez, M. *et al.* Mechanical and chemical unfolding of a single protein: a comparison. *Proc. Natl Acad. Sci. USA* **96,** 3694–3699 (1999).
8. Lu, H. & Schulten, K. Steered molecular dynamics simulations of force-induced protein domain unfolding. *Proteins Struct. Funct., Genet.* **35,** 453–463 (1999).
9. Izrailev, I., Stepaniants, S., Balsera, M., Oono, Y. & Schulten, K. Molecular dynamics study of unbinding of the avidin-biotin complex. *Biophys. J.* **72,** 1568–1581 (1997).
10. Soteriou, A., Clarke, A., Martin, S. & Trinick, J. Titin folding energy and elasticity. *Proc. R. Soc. Lond. B* **254,** 83–86 (1993).
11. Politou, A. S., Thomas, D. J. & Pastore, A. The folding and stability of titin immunoglobulin-like modules, with implications for the mechanism of elasticity. *Biophys. J.* **69,** 2601–2610 (1995).
12. Politou, A. S., Gautel, M., Improta, S., Vangelista, L. & Pastore, A. The elastic I-band region of titin is assembled in a "modular" fashion by weakly interacting Ig-like domains. *J. Mol. Biol.* **255,** 604–616 (1996).
13. Improta, S. *et al.* The assembly of immunoglobulin-like modules in titin: implications for muscle elasticity. *J. Mol. Biol.* **284,** 761–777 (1998).
14. Granzier, H., Helmes, M. & Trombitas, K. Nonuniform elasticity of titin in cardiac myocytes: A study using immunoelectron microscopy and cellular mechanics. *Biophys. J.* **70,** 430–442 (1996).
15. Granzier, H., Kellermayer, M., Helmes, M. & Trobitas, K. Titin elasticity and mechanism of passive force development in rat cardiac myocytes probed by thin-filament extraction. *Biophys. J.* **73,** 2043–2053 (1997).
16. Trombitas, K. *et al.* Titin extensibility in situ: entropic elasticity of permanently folded and permanently unfolded molecular segments. *J. Cell Biol.* **140,** 853–859 (1998).
17. Labeit, S. & Kolmerer, B. Titins: giant proteins in charge of muscle ultrastructure and elasticity. *Science* **270,** 293–296 (1995).
18. Labeit, S., Kolmerer, B. & Linke, W. A. The giant protein titin. Emerging roles in physiology and pathophysiology. *Circ Res.* **80,** 290–294 (1997).
19. Linke, W. A., Stockmeier, M. R., Ivemeyer, M., Hosser, H. & Mundel, P. Characterizing titin's I-band Ig domain region as an entropic spring. *J. Cell Sci.* **111,** 1567–1574 (1998).
20. Gautel, M. & Goulding, D. A molecular map of titin/connectin elasticity reveals two different mechanisms acting in series. *FEBS Lett.* **385,** 11–14 (1996).
21. Rief, M., Pascual, J., Saraste, M. & Gaub, H. E. Single molecule force spectroscopy of spectrin repeats: low unfolding forces in helix bundles. *J. Mol. Biol.* **286,** 553–561 (1999).
22. Marszalek, P. E., Oberhauser, A. F., Pang, Y.-P. & Fernandez, J. M. Polysaccharide elasticity governed by chair-boat transitions of the glucopyranose ring. *Nature* **396,** 661–664 (1998).
23. Lu, H., Isralewitz, B., Krammer, A., Vogel, V. & Schulten, K. Unfolding of titin immunoglobulin domains by steered molecular dynamics simulation. *Biophys. J.* **75,** 662–671 (1998).
24. Evans, E. & Ritchie, K. Strength of a weak bond connecting flexible polymer chains. *Biophys. J.* **76,** 2439–2447 (1999).
25. Hermans, J., Berendsen, H. J. C., Van Gunsteren, W. F. & Postma, J. P. M. A consistent empirical potential for water-protein interactions. *Biopolymers* **23,** 1513–1518 (1984).
26. Oberhauser, A. F., Marszalek, P. E., Erickson, H. P. & Fernandez, J. M. The molecular elasticity of the extracellular matrix protein tenascin. *Nature* **393,** 181–185 (1998).
27. Florin, E. L. *et al.* Sensing specific molecular interactions with the atomic force microscope. *Biosens. Biolelectr.* **10,** 895–901 (1995).
28. Nelson, M. *et al.* NAMD—A parallel, object-oriented molecular dynamics program. *Int. J. Supercomputer Applications and High Performance Computing.* **10,** 251–268 (1996).
29. Brunger, A. *X-PLOR, Version 3.1: A System for X-ray Crystallography and NMR* (Yale Univ., New Haven & London, 1992).
30. Humphrey, W. F., Dalke, A. & Schulten, K. VMD-visual molecular dynamics. *J. Mol. Graphics* **14,** 33–38 (1996).

Acknowledgements

We thank M. Gautel for a gift of the I27-134/pET8c plasmid, and T. Fisher for comments on the manuscript. This work was supported by NIH and NSF grants to J.M.F., P.E.M. A.F.O. and K.S., and by the Roy J. Carver Charitable Trust to K.S.

Correspondence and requests for materials should be addressed to J.M.F. (e-mail: fernandez-julio@mayo.edu).